CHALMERS
UNIVERSITY OF TECHNOLOGY

Finite element analyses of FRP-strengthened concrete beams with corroded reinforcement

Engineering Structures 257 (2022) 114007

Contents lists available at ScienceDirect

Engineering Structures

journal homepage: www.elsevier.com/locate/engstruct

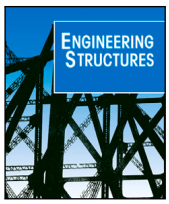

Finite element analyses of FRP-strengthened concrete beams with corroded reinforcement

Milan Gotame [a], Carl Lindqvist Franklin [a], Mattias Blomfors [b], Jincheng Yang [a], Karin Lundgren [a,*]

[a] Department of Architecture and Civil Engineering, Chalmers University of Technology, SE 412 96, Gothenburg, Sweden
[b] Bridge and Analysis group, Norconsult AB, SE 417 55, Gothenburg, Sweden

ARTICLE INFO

MSC:
00-01
99-00

Keywords:
Reinforced concrete structures
Finite element analysis
Corrosion
Fibre-reinforced polymer
CFRP
GFRP
Strengthening
Cracks
Interface
U-jacket

ABSTRACT

Existing deteriorated reinforced concrete (RC) structures need strengthening to extend service life. Fibre reinforced polymer (FRP) has been widely used to strengthen sound structures, but its application on damaged concrete structures still needs to be investigated. This paper presents non-linear finite element analyses conducted to assess the flexural behaviour of corrosion-damaged RC beams strengthened with externally bonded FRP. Beams in four different categories were analysed: a reference beam, a corroded but non-strengthened beam, and corroded beams strengthened with glass FRP (GFRP) and carbon FRP (CFRP) respectively. Furthermore, the strengthened beams were modelled with different modelling choices to investigate the effectiveness of FRP applied to the beam soffit and as U-jackets. Pre-loading and corrosion-induced cracks were incorporated by reducing the tensile strength of concrete elements at crack locations. Average and pitting corrosion were incorporated by reducing the cross-sectional area of the reinforcement corresponding to the measured corrosion levels. Interface elements were used to simulate the bond between FRP and concrete. The modelling methods were validated against experimental results. It was found that modelling of pitting corrosion, especially the location of pits, lengths and number of pits considered, were influential in predicting the load and deformation capacity of beams. A CFRP plate at the beam soffit, combined with inclined U-jackets at its ends of the CFRP plate provided sufficient flexural strengthening. Thus, intermediate U-jackets did not further increase the load-bearing capacity for the studied beam geometry and corrosion damages. However, with a GFRP sheet at the beam soffit, both inclined and intermediate U-jackets were needed to provide full utilisation of the GFRP sheet for the studied beam geometry. In further studies of the effectiveness of the strengthening methods, it is recommended to investigate beams of varying dimensions, corrosion patterns and levels, and FRP spacing and dimensions.

1. Introduction

Concrete has been a widely utilised material in structures over 150 years, due to its low cost, low need for maintenance, longevity, fire performance and stiffness [1]. Existing concrete structures built in the mid-to-late 1900s display increasing signs of deterioration due to adverse environmental conditions resulting in reduced capacity [1]. The most common cause of degradation of reinforced concrete (RC) structures is chloride-induced corrosion [2]. Corrosion of reinforcement degrades concrete structures in several ways. Pitting corrosion causes local reduction of the cross-sectional area of the reinforcement, reducing its yielding and ultimate capacities as well as its ductility [3,4]. The corrosion products occupy a larger volume than the original steel. This introduces splitting stresses, and, ultimately, results in spalling of the concrete cover and weakening of the bond between the concrete and reinforcement [5]. The latter may cause anchorage failure and reduced load-carrying capacity. Furthermore, variables such as higher volumes of commuter and cargo activity, and heavier vehicles have increased the load on existing structures throughout the world [1], creating a need for increased capacity. To reduce the cost and environmental impacts of new constructions, it is vital (for society and the environment) to be able to strengthen structures such as bridges and buildings.

Strengthening with fibre-reinforced polymers (FRP) is a well-accepted technique for increasing the capacity of concrete structures [6]. There has been much research into strengthening of sound structures with FRPs [1,7]. However, the need to be able to strengthen deteriorated structures has increased, and research is needed to know how to apply this to the strengthening of corrosion-damaged structures. Due to the high strength-to-weight ratio and high modulus of elasticity, externally bonded FRPs in the beam soffit are easy to handle and

* Corresponding author.
E-mail address: Karin.Lundgren@chalmers.se (K. Lundgren).

https://doi.org/10.1016/j.engstruct.2022.114007
Received 1 October 2021; Received in revised form 1 February 2022; Accepted 7 February 2022
Available online 9 March 2022

effective in improving structural behaviour [1]. However, for heavily corroded RC structures, externally bonded FRPs might not improve the load capacity, stiffness and ductility capacity effectively due to damaged concrete cover [8–10]. Triantafyllou [11] and Al-Saidy [8] suggested doing a patch repair of the damaged concrete cover before applying FRP plates, to improve the structural performance of the corrosion-damaged RC structures. In practice, a patch repair might not be feasible for RC structures due to its vulnerability to the removal of concrete cover and labour-intensive uneconomical characteristics. Thus, there is a need for alternative strengthening techniques. It has been shown that the combination of transverse FRP wraps/U-jackets wrapped around the beam with FRP plates, can improve the flexural performance without needing a patch repair [11].

Nowadays, the finite element (FE) method (FEM) is commonly used in the structural analysis of RC structures. To model corrosion-damaged concrete beams, the damage (both in the form of corrosion-induced cracks and reductions in reinforcement area) need to be included. According to Blomfors [12,13], the weakening of concrete elements at the location of cracks in an FEA model gives reasonable results when compared with test results, in terms of load vs deflection and ultimate capacity. Considering that pitting corrosion has a major impact on the reduction of ultimate and deformation capacity of a beam [14], modelling local corrosion is highly important in accurately predicting the capacity of corrosion-damaged RC structures. The local pitting and general corrosion of steel reinforcement can be modelled by reducing its cross-sectional area [15].

Previously, two-dimensional (2D) [16–18] and three-dimensional (3D) [13,19–22] FE modelling have been used to analyse sound, corroded and strengthened concrete beams. Even though 2D symmetrical FE modelling can lead to good results [16,17], 3D FE modelling may be needed for reasons such as: (i) the potential corrosion effects are typically 3D in nature (ii) for a particular beam size, the assumption of plane stress or plane strain may not be completely true and (iii) the FRP strengthening may not be applied to the entire width of the beam. Normally, FRP strengthening is modelled as shell elements with an orthotropic material, or as brick elements defined with an isotropic 3D material representing the adhesive and unidirectional and bi-directional smeared reinforcement of fibres [23]. The bond behaviour between the concrete and FRP has an influence on the debonding of FRP and stiffness of strengthened RC structures. Researchers have used different methods to model the bond behaviour between concrete and FRP in non-linear finite element analyses (NLFEA). According to current literature, two different methods have been found to be more common: (i) full bond without failure/damage [24]; (ii) behaviour with limited strength and damage evolution [25,26]. In terms of how to assign the bond behaviour, we can (i) define constitutive law directly between two interfacial surfaces or (ii) use elements to model the bond line and assign the law to interfacial elements [27,28]. Between these two methods, the interface elements have most commonly been used to simulate the interaction between concrete and FRP. In this method, the interfacial properties can be assigned by defining the constitutive bond stress versus slip relationship or shear traction–separation law [27,28]. Chen et al. [29] concluded that the bond behaviour between the concrete and FRP is important to accurately predict the failure and crack pattern of strengthened RC structures. Several other researchers have also applied NLFEA to FRP-strengthened RC beams, and shown that the failure mode and behaviour can be accurately predicted when the bond between concrete and FRP is properly included [21,22,30,31].

FE analyses of FRP-strengthened beams with corroded reinforcement thus includes several major challenges. In addition to modelling of cracking reinforced concrete, special consideration needs to be taken on how to include the corrosion damages and how to model interaction between the concrete and the FRP strengthening. Thus, modelling methods need to be developed and validated to experimental results. In this research work, FE models were developed and the analyses were validated to experiments carried out by Yang [14]. The corrosion levels, material properties of concrete, reinforcement and FRPs were used according to measurements made by Yang. Based on the validated FE models, different examples of FRP composite applications were analysed to investigate their effects on flexural responses and failure modes.

2. Overview of analysed experiments

The RC beams analysed in this FEA study were tested in four-point bending until failure by Yang [14]. The first test group, RN, included two sound beams, non-strengthened to act as reference. Among the deteriorated beams, two were non-strengthened (DN), three were strengthened with GFRP (DG) and three were strengthened with CFRP (DC). This section presents an overview of the experiments. For a more detailed information about the tests, see Yang [14,32].

The tested RC beam specimens are of 2.1 m length, 225 mm height and 150 mm width, as shown in Fig. 1(a). The concrete mix has proportions of cement:sand:gravel:water = 1:2.46:1.90:0.43 by weight. Section 3.3 presents the properties of concrete and reinforcement at the time of structural failure tests. The damaged beams were pre-cracked by three-point bending, followed by 75 days of accelerated corrosion of the tensile reinforcement bars at the mid-600 mm zone. The three-point bending and accelerated corrosion resulted in transverse bending cracks and longitudinal corrosion-induced cracks. At the mid-span, the crack width was in the range of 0.7 to 1.9 mm. The corrosion-induced cracks were propagated within the mid-900 mm region. Fig. 1(b) shows how the FRPs were bonded externally to the concrete surface. The 1500 mm long GFRP sheet and CFRP plate with cross-sections of 150x3.03 mm^2 and 100x1.45 mm^2 respectively, were attached to the beam soffit. After 48 h of curing, CFRP U-jackets were installed on the DG and DC beams, see Fig. 1(b). The vertical U-jackets have one layer of CFRP fabric, whereas the 45°inclined U-jackets have three layers of CFRP fabric. After bonding of the FRPs, the beams were cured for four weeks prior to the four-point bending tests.

The beams with an effective span of 1.8 m were tested in four-point bending. Variable differential transformers (LVDT) were used to measure the net deflection at the middle of the beam and at the two supports. In the FRP composites, the axial strains at critical positions were measured by strain gauges (SG5, SG6), see Fig. 1(b). After the four-point bending tests, the tensile reinforcement bars were extracted from the beams and the corrosion levels were measured using 3D optical scanning [14].

3. Numerical modelling

The flexural behaviour of reference, corrosion-damaged and FRP-strengthened RC beams tested by Yang [14] was studied using 3D NLFEA in DIANA 10.4 [33]. This section presents the FE modelling approaches are presented.

3.1. Summary of analyses carried out

For ten tested specimens, one beam from each of the four different categories was analysed. A reference beam (RN1), a corroded but non-strengthened specimen (DN1) and corroded beams strengthened with GFRP and CFRP (DG1 and DC1 respectively) were modelled using different modelling choices. An overview of these analyses and the different modelling choices is presented in Table 1.

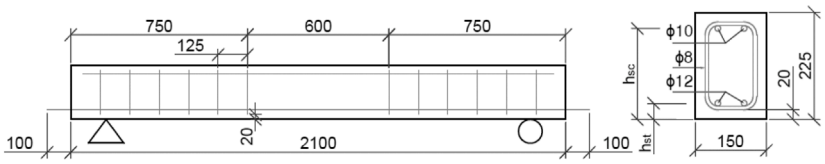

(a) Beam geometry and cross-section [14]. Here, h_{st} and h_{st} are the level of the bottom and top reinforcements from the bottom surface of the beam, respectively, according to Yang [14].

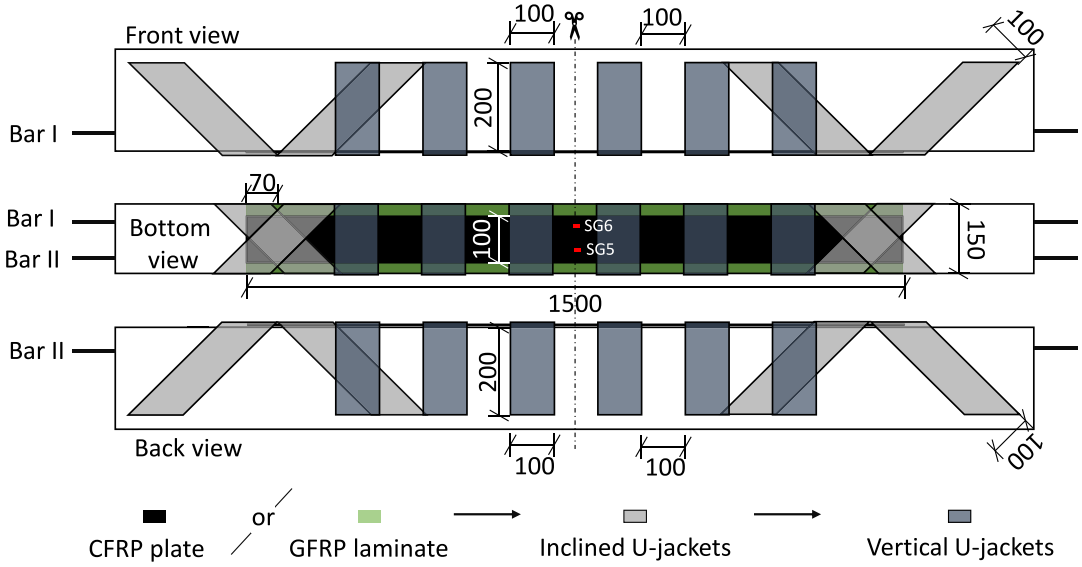

(b) FRP strengthening method used by Yang to the corrosion-damaged concrete beams [14].

Fig. 1. Overview of experiments.

3.2. Beam idealisation and meshing

Since the corrosion damage for the damaged RC beams was not symmetrical, they were modelled with their complete geometry. The reference beam was used as a basis, and was further developed for modelling of the corroded and strengthened beams. The idealised reference beam for the 3D FE model is shown in Fig. 2. The concrete was modelled using 3D solid continuum elements of brick, tetrahedron, pyramid, and wedges (HX24L, TE12L, PY15L, TP18L, respectively), all with linear interpolation and normal gauss integration. The average size of element lengths was set to 20 mm, fulfilling the recommendation of using a minimum of $(\frac{l}{50}, \frac{h}{6}, \frac{b}{6})$, as suggested by Hendriks [34]. Longitudinal reinforcement bars were modelled as beam elements, which were connected to surrounding concrete by interface properties as described in Section 3.3. However, the top rebars and stirrups were assigned as embedded reinforcement, assuming full interaction with the concrete. In the FE model, the loading and support plates were modelled as 25 mm thick plates with solid elements. Thin wooden plates, modelled using solid elements, were applied under them to avoid stress concentration on the concrete near the plates. The interface between the concrete beam and steel loading and support plates was modelled using Q24IF elements. The centre nodes along the support plates were restricted to displace vertically at both left and right support plates, and also restricted horizontally at the right support. The load distribution beam, used in the tests, was idealised with beam elements (L12BEA). The end nodes of the loading beam were tied to the centre lines of the loading plates in their vertical displacement. Furthermore, the centre node of the loading beam was restricted to displacing horizontally to ensure the stability of the loading beam. The distance between the centres of the loading plates was 600 mm. The load was applied as deformation at the midpoint of the loading beam, see Fig. 2.

3.3. Models for concrete, reinforcement and their interaction

Table 2 shows the material properties of the concrete used in the FEA. These are based on compression and wedge split tests conducted by Yang [32]. Concrete cracking was modelled using a smeared rotating crack model based on the total strain, as described in [33]. The crack band width was assumed as $\sqrt[3]{V}$, where V is the volume of a 3D concrete element, as proposed by Rots [35]. This crack band width was later verified against approximate lengths of zones with localised strains in the analysis. For the reference beam, the tensile strength of the concrete elements at the mid-section, see Fig. 2, was reduced by 20% to promote strain localisation; this largely improved the convergence. The tensile behaviour of concrete was characterised by the tensile strength–strain relationship, introduced by Hordijk [36]. The behaviour of concrete in compression was taken into account using a parabolic compression curve, according to Feenstra [37], with a softening branch. The softening branch of the compression curve is based on the compressive fracture energy. A reduction factor of 0.6 due to lateral cracking was used, according to Vecchio & Collins [38]. To simulate the behaviour of reinforcement in the FE analyses, the tensile stress–strain curve was given as an input. The stress–strain properties of the steel reinforcement bars were obtained from standard tensile tests conducted by Yang [32]. The curves fitting the average of six tensile tests of both the top and bottom rebars were used as input in the FE analyses, for detailed information, see [39].

The interaction between concrete and bottom reinforcement was modelled using a bond stress–slip relationship according to *fib* Model

Table 1
Overview of FE analyses.

Beam	FEA model	Description	F_u[a] [kN]	Δ_u[b] [mm]	Failure mode
RN1	RN1_FEA	Reference RC beam	88.8	53.0	Concrete crushing
DN1	DN1_GC_FEA	Reference beam modified to damaged beam with only general corrosion corresponding to DN1 beam	76.0	64.1	Concrete crushing
	DN1_FEA	Three major corrosion pits in each rebar	50.8	17.9	Rebar rupture
	DN1P_FEA	One major corrosion pit in each rebar	51.4	9.9	Rebar rupture
	DN1PE_FEA	One major corrosion pit in each rebar with extended yield penetration length	51.4	9.1	Rebar rupture
DG1	DG1N_FEA	Corroded but non-strengthened	50.9	10.4	Rebar rupture
	DG1S_FEA	Corroded, strengthened with GFRP sheet only	94.5	14.7	Concrete separation
	DG1IU_FEA	Corroded, strengthened with GFRP sheet and inclined U-jackets	111.0	18.6	Anchorage failure
	DG1NLI_FEA	Corroded, strengthened with GFRP sheet, vertical and inclined U-jackets, non-linear interface for U-jackets	112.0	18.0	Anchorage failure
	DG1_FEA	Corroded, strengthened with GFRP sheet, vertical and inclined U-jackets, linear interface U-jackets	131.0	22.8	GFRP rupture
DC1	DC1N_FEA	Corroded, but non-strengthened	49.6	10.1	Rebar rupture
	DC1P_FEA	Corroded, strengthened with CFRP plate only	119	11.8	Anchorage failure
	DC1IU_FEA	Corroded, strengthened with CFRP plate and inclined U-jackets	160	14.5	Anchorage failure
	DC1_FEA	Corroded, strengthened with CFRP plate, vertical and inclined U-jackets	168	14.6	Anchorage failure

[a] F_u – total ultimate load applied.
[b] Δ_u – deflection at mid-span of beam corresponding to the ultimate load.

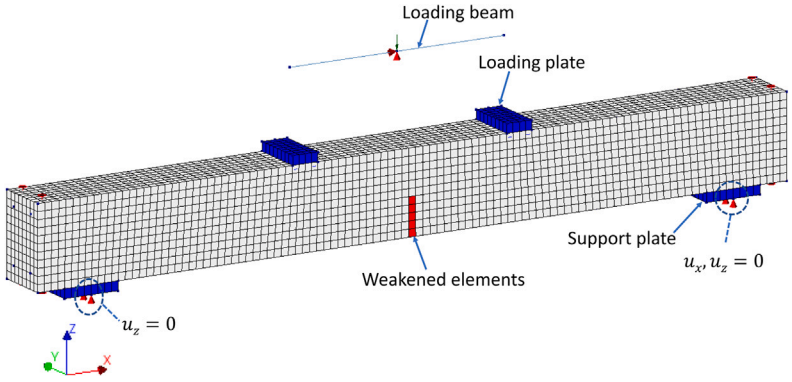

Fig. 2. 3D FE mesh of the reference beam (FE model RN1).

Code 2010 [40], assuming "Good" bond condition and "Pull-Out" failure condition. The effect of corrosion on the bond–slip relationship was not considered, as it is of minor importance for the analysed beams. Note that this effect is important for other cases, such as when anchorage or shear failure takes place (note also that corrosion may change the failure mode to these). This effect can then be included either by modifying the bond–slip behaviour, or by use of a frictional model between the steel and the concrete, see [13]. The normal stiffness was set to 10^{13} N/m^3. Full interaction was assumed between top reinforcement and concrete, as well as between stirrups and concrete.

Table 2
Material properties of concrete used in the non-linear analyses.

Concrete properties	Value	Reference	Test
Mean compressive strength $f_{cm} = 0.8 f_{cm.cube}$	63 [MPa]	[32,40]	$f_{cm.cube}$[a]
Mean tensile strength $f_{ct} = 2.12 ln(1 + 0.1 f_{cm})$	4.21 [MPa]	[40]	–
Young's modulus E_{cm}	33.3 [GPa]	[32]	$E_{cm.cylinder}$[b]
Tensile fracture energy G_F	134 [N/m]	[32]	Wedge[c]
Compressive fracture energy $G_C = 250 G_F$	33500 [N/m]	[40]	–

[a] $f_{cm.cube}$ – from standard compressive test of concrete cubes (side length 150 mm).
[b] $E_{cm.cylinder}$ – from standard test of cylindrical specimens of 100 mm diameter and 200 mm height.
[c] Wedge – from wedge splitting test.

3.4. Implementation of pre-existing cracks

For beams in the categories DN1, DG1 and DC1, the cracks induced due to pre-loading (transverse cracks) and corrosion (longitudinal cracks) were incorporated by reducing tensile strength and fracture energy for the corresponding concrete elements, as suggested by Blomfors et al. [12,13]. The reduction was based on the measured crack widths, w_c. The reduced tensile properties of the weakened

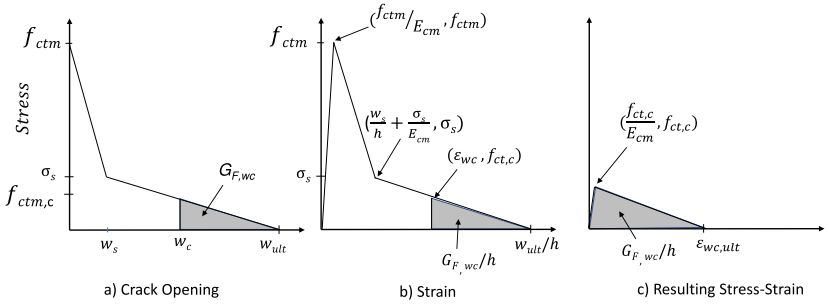

Fig. 3. Principle of deriving reduced stress versus strain curve for weakened concrete using the crack widths (w_c), proposed by Blomfors [12]: (a) Bi-linear stress-crack opening relationship [41] (b) Stress–strain relationship, using the crack band width h, (c) The resulting stress–strain relationship for the weakened elements. Here, $f_{ct,c}$ is the reduced tensile stress, $G_{F,wc}$ is the reduced residual fracture energy and $\varepsilon_{wc,ult} = \frac{w_{ult}-w_c}{h}$ for $w_c > w_s$.

concrete elements were determined from the corresponding crack width w_c in a bilinear mode-I stress-to-crack width relationship with a break point, according to Wittmann et al. [41], see Fig. 3(a), which was characterised by σ_s = 1.05 MPa, w_{ult} = 0.159 mm [40], and w_s = 0.0239 mm. This is a simplified way to include existing damage, and is specially well suited when inspection results of existing structures are available. At prediction of future damages, several models for development of corrosion-induced cracking exist, e.g. [42,43].

For each of the transverse cracks, the crack width was assumed to be constant along the width of the beam. Moreover, the longitudinal cracks were assumed to have the same crack width throughout their crack length. For those crack widths larger than the breaking point in the bilinear mode-I stress-to-crack width curve, the widest crack width was chosen. Furthermore, for cracks with a width close to or larger than the ultimate crack width (w_{ult}), a tensile strength corresponding to $0.99w_{ult}$ was assumed. Fig. 3 shows how the reduced tensile stress versus strain was calculated. In FE modelling, this was given as input for the weakened concrete element rows. For the weakened elements, the strain localisation was assumed over an element, so that h = 20 mm.

Fig. 4 shows a 3D view of weakened concrete elements corresponding to pre-existing cracks, in DN1 and DC1 beams. In general, the corrosion-induced cracks, on the bottom face of the beams, were assumed to extend to as much as twice the level of the tensile rebars from the beam soffit. Moreover, for corrosion-induced cracks at the side face, elements at the level of the tensile rebars were weakened. These cracks were assumed to extend to twice the effective cover of the tensile rebar along the width of beam.

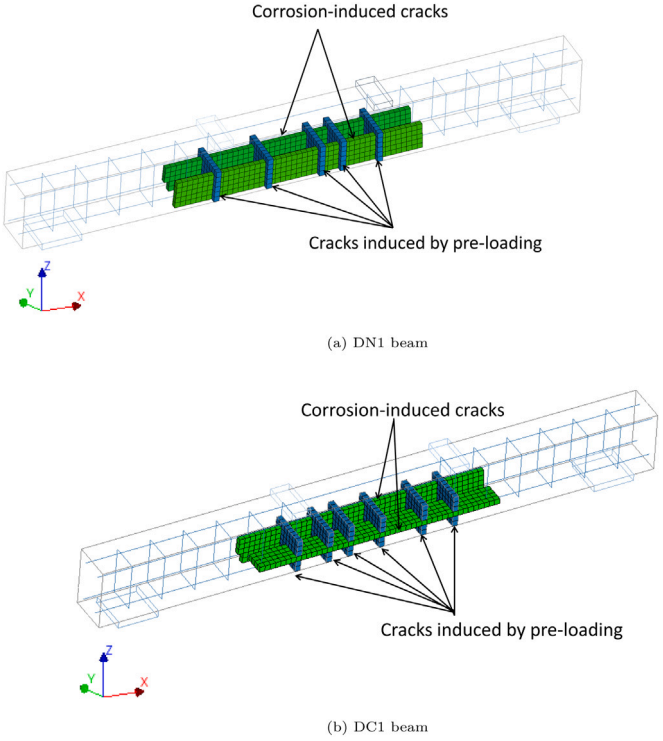

Fig. 4. 3D view of weakened elements for cracks induced by pre-loading and corrosion.

3.5. Modelling of corrosion damage in rebars

The measured general and pitting corrosion characteristics were implemented in the FE model by reducing the cross-sectional area of the corroded bottom tensile rebars. The general corrosion was considered by reducing the cross-sectional areas of the rebars to correspond with the average corrosion level in the mid 900 mm. The pitting corrosion was considered by further reducing the cross-sectional areas of the bottom rebars at the locations of major pits, according to the 3D scanned values. At loading, localised strains are generated at the location of a severe corrosion pit [4]. At yielding, the localised strains will spread within a certain region, here denoted as the yield length, l_y, but limited by the fact that rupturing of the rebar will occur at the pit before yielding takes place outside the yield length. By looking at the equilibrium of a uniaxially loaded bar with varying corrosion levels and a corrosion pit with maximum corrosion level (μ_{max}), the corrosion level at the end of yield length, μ_p, can be calculated as:

$$\mu_p = 1 - (1 - \mu_{max}) f_u / f_y \tag{1}$$

where f_u and f_y are the ultimate and yield strength of the rebars and μ_{max} is the maximum corrosion level of the pit:

$$\mu_{max} = 1 - A_{corr.min}/A_{ini} \tag{2}$$

where A_{ini} is the cross-sectional area of a rebar before corrosion and $A_{corr.min}$ is the minimum cross-sectional area of the rebar at pit after corrosion, extracted from 3D-scanning data. Thereafter, the cross-sectional area of the rebar just outside the yield length, A_p, was calculated by using equation:

$$A_p = (1 - \mu_p) A_{ini} \tag{3}$$

The expected yield length (l_y) was estimated by measuring the length of the pit with corrosion levels greater than μ_p using the 3D scanned data of the rebars, see Fig. 5. Moreover, Fig. 5 presents how the average and local corrosion were implemented in the FE model for bar I of the DN1 beam.

As indicated in Fig. 5 (bottom), the cross-sectional area of the rebar elements were reduced along length l_y at the location of pits in the FE model. However, the yield length was not always equal to an integer multiple of the element length, l_e. Accordingly, the closest integer multiple (n) was chosen, and the ultimate and rupture strain was modified to:

$$\varepsilon_{mod} = \varepsilon_{ini} l_y / n l_e. \tag{4}$$

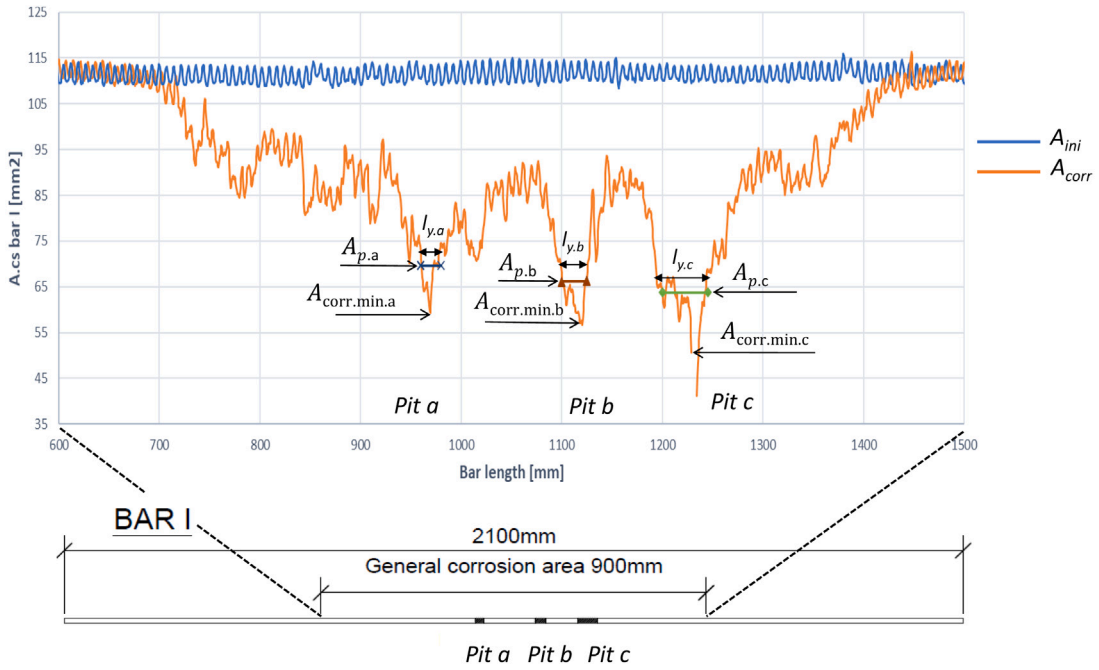

Fig. 5. Example of how the yield length (l_y) was estimated using the 3D scanning data of bar I of DN1 beam, plus how this was implemented in the FE model. 3D scanned data shows the cross-sectional area of the rebar before and after corrosion. $A_{initial}$ and A_{corr} are cross-sectional areas of rebar before and after corrosion, $A_{corr.min.a}$, $A_{corr.min.b}$ and $A_{corr.min.c}$ are the minimum cross-sectional areas and $A_{p.a}$, $A_{p.b}$ and $A_{p.c}$ are cross-sectional areas of a rebar at the end of yield penetration, corresponding to Pit a, b and c respectively.

where ε_{ini} is the initial strain of the rebars.

A number of models were analysed to study the effects of the number of pits and how close those pits were to each other in the different rebars. Furthermore, the authors investigated how adding "neighbouring" elements to the pit (thus increasing the yield length) affects the deformation capacity of the beam. These neighbouring elements were assigned the cross-sectional area of A_p. A detailed explanation of the incorporation of the corrosion damages may be found in [39].

3.6. Modelling of FRP

The FRPs were modelled as 3D plane stress (3D membrane) quadrilateral elements (Q12GME elements). Isotropic material properties were assigned to the GFRP sheet, CFRP plate and inclined U-jackets, while orthotropic material properties were assigned for the unidirectional vertical U-jackets, see Table 3. The stiffness in the weak direction, x-direction in Fig. 6, of the vertical U-jackets was assumed to be the same as the epoxy which was used between the CFRP plate and the concrete. The linear stress–strain relationship of the FRP was implemented in FE analyses as a linear elastic material with a brittle failure when reaching the tensile strength. The tensile strength for the FRP material was calculated by multiplying the elastic modulus (E_f) by the rupture strain (ε_{fu}).

Fig. 6 presents the meshing of the FRPs for the DG1 beam, with the different geometries indicated by arrows. The average element size of the FRP was set to 20 mm to align with the concrete. However, a mesh size of 5 mm was chosen for CFRP plate in beam category DC1, as recommended by Kalfat [23].

The interface properties between FRPs and concrete were modelled as 3D structural plane interface (Q24IF elements). The non-linear interface properties were modelled by the bi-linear bond stress–slip relationship proposed by Lu et al. [28], characterised by s_0 = 0.0611 mm and 0.07 mm, s_f = 0.149 mm and 0.182 mm, τ_{max} = 4.71 MPa and 5.74 MPa for GFRP-concrete and CFRP-concrete interfaces respectively. The same bond stress–slip relationships were considered for the connection between U-jackets to concrete and U-jackets to CFRP plate. However, for the DG1 beam, one additional analysis was carried out; assuming linear properties corresponding to the stiffness in the first segment of the bi-linear relationship.

3.7. Iterative scheme

The NLFEA of RC beams were done by applying deformation-controlled loading, as shown in Fig. 2. For the reference beam, the deformation was applied in 500 steps of 0.05 mm followed by 400 steps of 0.1 mm. For the analyses of deteriorated (DN1) and strengthened (DG1 and DC1) beams, the deformation was applied in 250 steps of 0.02 mm followed by 500 steps of 0.05 mm. The BFGS (Broyden, Fletcher, Goldfarb, and Shanno) method was used to perform equilibrium iteration [33]. The maximum number of iterations was set to 400 to achieve convergence. As suggested by Hendriks, an energy norm of 0.001 and a force norm of 0.01 were implemented as tolerance limits for convergence in analysis of RN1 and DN1 beams [34]. However, for the analysis of beams under the DC1 category, the energy norm limit was set to 0.01 to achieve the convergence.

4. Results and discussion

This chapter presents the results of the FE analyses with different modelling choices. The flexural behaviour of four beams (RN1, DN1, DG1 and DC1) are presented and compared with the test results. The effects of pitting corrosion on the deformation and ultimate capacity of the RC beams are also presented, in terms of load versus mid-span deflection curves. In addition to the tested beams, the results of analyses with different modelling choices (see Table 1), are presented to study the effectiveness of the FRP strengthening methods in improving the ultimate load and deformation capacity.

4.1. Behaviour in bending

The flexural behaviour of four beams from experiments and FEA are shown in Fig. 7 and Table 4. The FE analyses were able to capture the same failure mode as in the experiments, see Table 4. Failure due to concrete crushing after yielding of tensile reinforcement caused the flexural failure of the reference beam, see Fig. 8. In the FE analysis of the reference beam, crushing of the concrete was localised to one element row, which agreed with the assumed localisation zone, see

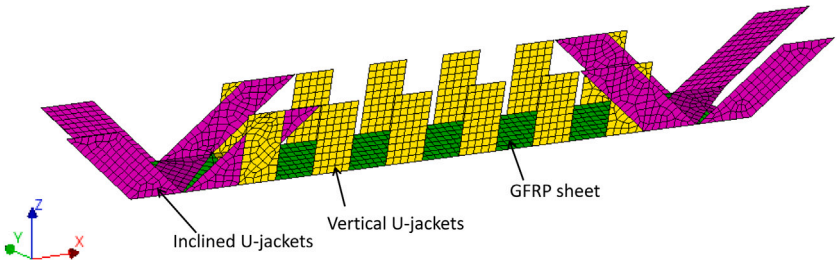

Fig. 6. Mesh for FRPs in the model of the DG1 beam.

Table 3
Dimensions and material properties of FRP composites [32].

FRP composites	width × thickness [mmxmm]	E_f [a] [GPa]	E_{fx} [b] [GPa]	E_{fy} [c] [GPa]	G_{xy} [d] [GPa]	ε_{fu} [e] [%]	ν [f] [mm]
GFRP laminate (isotropic)	150 × 3.03	20.2	–	–	–	1.82	0.2
CFRP plate (isotropic)	100 × 1.45	214	–	–	–	1.27	0.2
Inclined U-jacket (isotropic)	100 × 2.39	57.6	–	–	–	1.24	0.2
vertical U-jackets (orthotropic)	100 × 0.797	–	7.1	57.6	5	1.24	0.2

[a] E_f – isotropic modulus of elasticity.
[b] E_{fx} – modulus of elasticity in x-direction.
[c] E_{fy} – modulus of elasticity in y-direction.
[d] G_{xy} – shear modulus.
[e] ε_{fu} – ultimate tensile strain at rupture.
[f] ν – Poisson's ratio.

Fig. 8. As shown in Fig. 9, in the non-strengthened deteriorated beam, rupture of the bar at the left pit in the second (II) bottom rebar caused a brittle failure (FE model DN1_FEA). A brittle failure due to rupture of the GFRP sheet was found in DG1 beam, see Fig. 10 (FE model DG1_FEA). Furthermore, the DC1 beam failed due to a brittle anchorage failure at the end of the CFRP plate, see Fig. 11 (FE model DC1_FEA).

It is worth noting that the ultimate load capacity of the reference beam (RN1) was 88.8 kN in the FE analysis, which is 14% larger than the test result. This difference was carefully investigated. Analytical calculations were done to calculate the cracking, yielding, and the ultimate load of the reference beam. These agreed well with the FE results, see Fig. 7. A number of possible reasons for the discrepancies to the test results were investigated by confirming:

- beam height and placement of the reinforcement bars against test photos.
- force capacity for the bottom reinforcement bars with additional material tests.
- calibration of load cells used in beam and reinforcement testing.

However, no explanation was found for the discrepancies. The analyses of the strengthened beams agreed better with the tests results. Thus, when the FRPs were the main component providing stiffness for the beams, the results matched the tests better.

The crack patterns at a mid-span deflection of 9.39 mm were compared, based on DIC measurements during experiments and from FE analyses, see Fig. 12. As the cracks in the FE analyses were localised into one element row, the assumed crack bandwidth was validated. In RN1 beam, the cracks were well distributed over the mid-900 mm region, both in the experiment and the FE analysis. In the damaged beam, the crack width increased and cracks were localised to the mid-section in-between the loading plates. Both in FE analyses and tests, the application of FRPs suppressed the crack opening effectively, thereby reducing both the number and width of cracks.

4.2. Effects of corrosion

The effects of general and pitting corrosion were studied by analysing the beam of category DN1. As described, the analysis of the damaged beam (including the general and pitting corrosion) was able to predict the same failure mode as in the test; in other words, the rupture of the pitted rebars. The analysis including only general corrosion was developed from the RN1 beam by incorporating only general corrosion levels corresponding to DN1 beam measured by Yang [14] at mid-900 mm region (model DN1_GC_FEA). In this analysis, the load capacity was decreased compared to the reference beam, but the deformation capacity was not influenced, see Fig. 13.

By including the pitting corrosion, the load capacity was further decreased. Similar load capacity was found in all analyses, including pitting corrosion. However, the deformation capacity was found to be highly sensitive to the modelling of pitting corrosion, see Fig. 13. This was studied by trying different modelling choices for the corrosion pits. It was considered important to find a balance between having a simple and practical modelling approach for the corrosion pits and to have a response that was close to the test results. Three different modelling approaches were examined for modelling the pitting corrosion. It was found that the analysis with three major pits in each tensile rebar agreed best with the test results (model DN1_FEA). This analysis displayed a higher deformation capacity compared to the other ones. This was because it avoided premature failure of the pits in the rebars compared to the model with only one major pit at a critical section (models DN1P_FEA and DN1PE_FEA). Model DN1PE_FEA was similar to model DN1P_FEA but the yield length was extended by reducing

Table 4
Ultimate load capacity and failure modes of all beam specimens in experiments (EXP) and FEA.

Specimens	F_u [a] [kN]			Δ_u [b] [mm]			Failure mode
	EXP	FEA	Ratio	EXP	FEA	Ratio	EXP and FEA
RN1	77.7	88.8	1.14	46.7	53.0	1.13	CC[c]
DN1	41.5	50.8	1.22	16.3	17.9	1.10	RS[d]
DG1	135.8	131.0	0.96	20.1	22.8	1.13	RG[e]
DC1	170.8	168.0	0.98	16.4	14.6	0.89	AC[f]

[a] F_u - total ultimate load applied.
[b] Δ_u – corresponding deflection at mid-span of beam.
[c] CC – failure due to concrete crushing.
[d] RS – rupture of steel rebar.
[e] RG – rupture of GFRP sheet.
[f] AC – anchorage failure of CFRP plate.

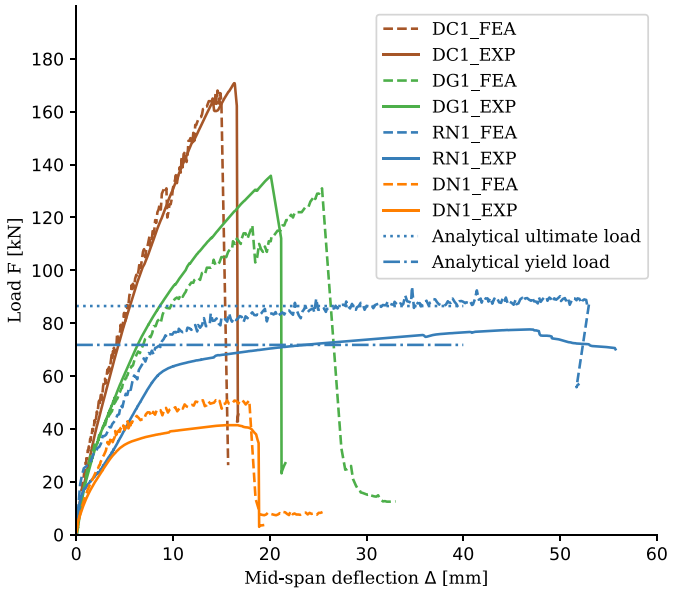

Fig. 7. Load versus mid-span deflection and FE analyses results compared with the experimental results..

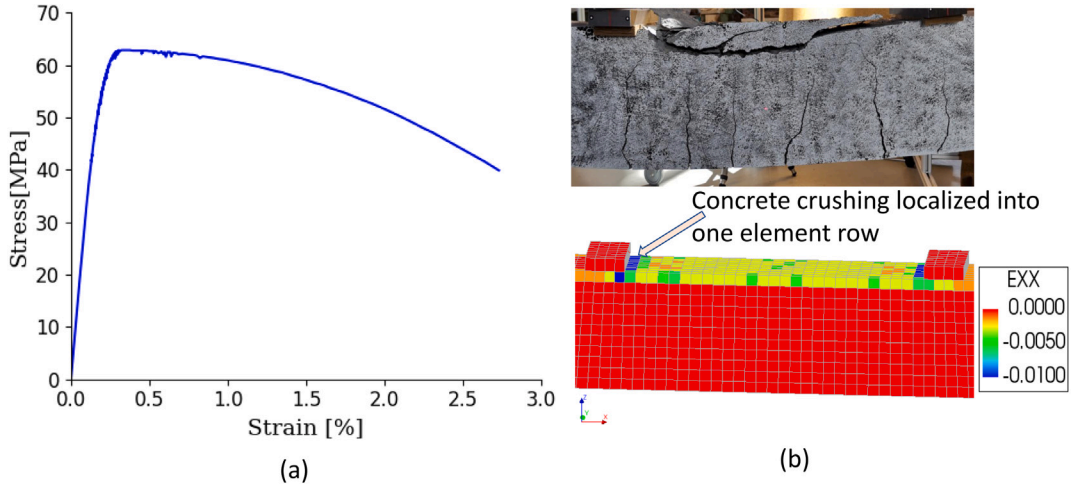

Fig. 8. Concrete compressive stress vs strain at one of the critical integration points in the analysis of RN1 beam. All elements in a row along the *y*-direction failed in the crushed state: (a) Stress vs strain at the critical integration point associated with the concrete element indicated in figure (b), (b) Failure of the RN1 beam due to concrete crushing and localisation of concrete crushing into one element row. The test photo shows crushing of concrete at failure.

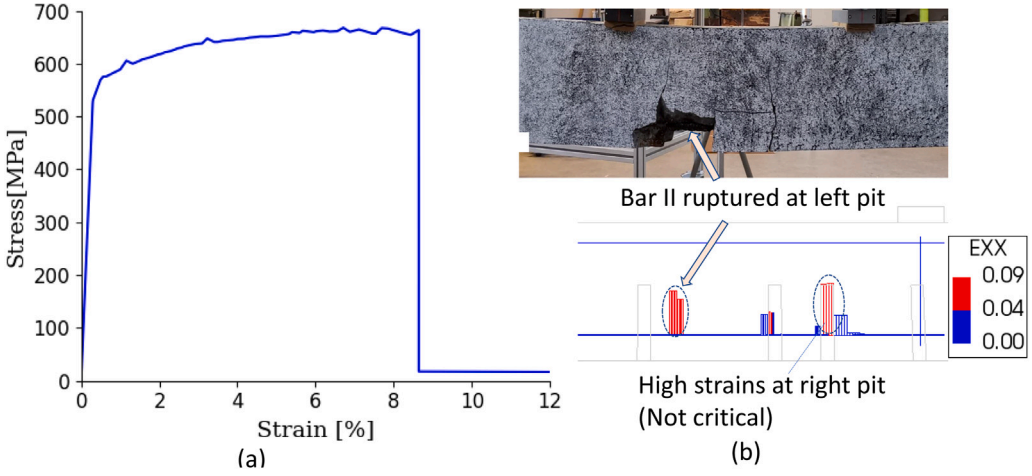

Fig. 9. Stress versus strain for tensile bar II at the critical pit of DN1 beam from FE analyses: (a) Stress versus strain at left pit, indicating failure of the beam, (b) Reinforcement element with high strain which initiated failure of the beam due to rupture. The experimental photo shows failure due to rupture of corroded tensile rebar.

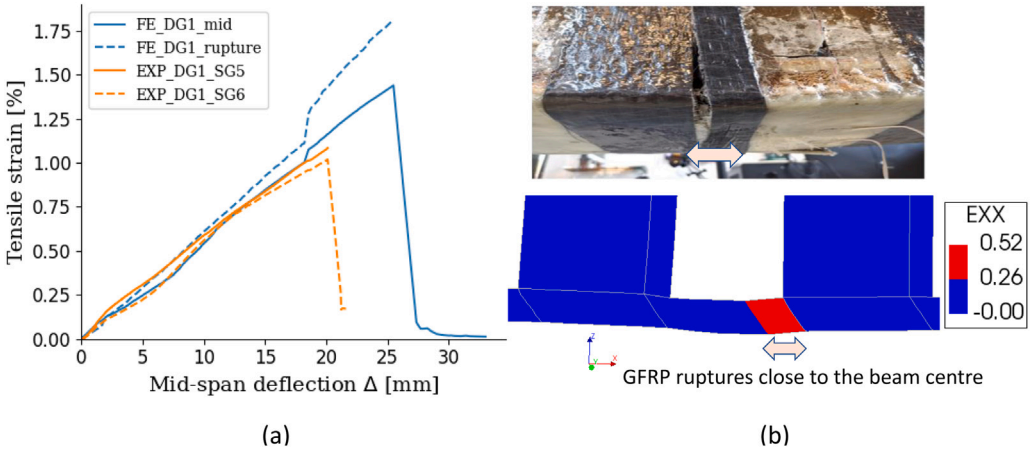

Fig. 10. Strain development for DG1 beam: (a) The strain versus mid-span deflection for GFRP sheet at an integration point corresponding to rupture at mid-section plus FE results compared to the test results, (b) Rupture of GFRP sheet from experiment and FE analysis.

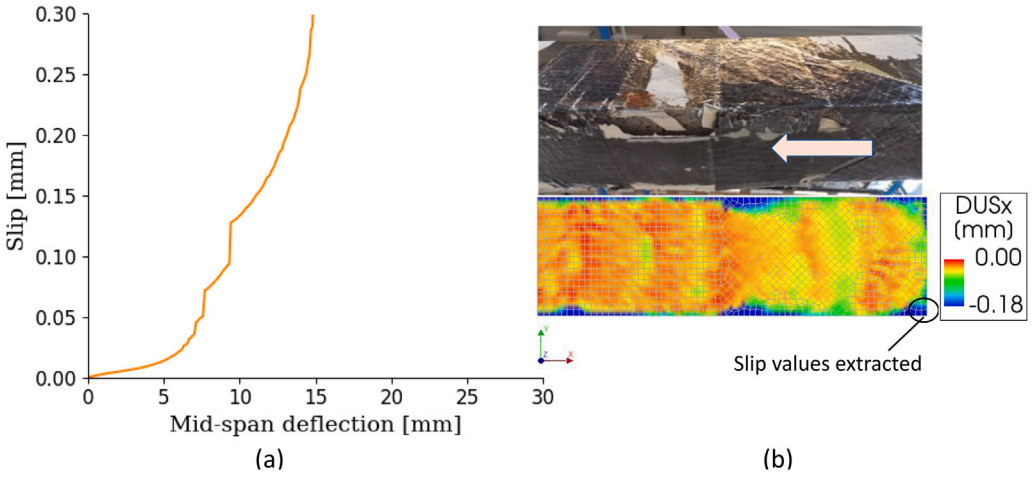

Fig. 11. (a) End slip versus mid-span deflection of CFRP plate in DC1 beam from FE analyses, (b) High slip values at the end of CFRP plate, indicating anchorage failure as in experiment. The test photo shows slip of the CFRP plate plus inclined U-jackets towards the centre of the beam.

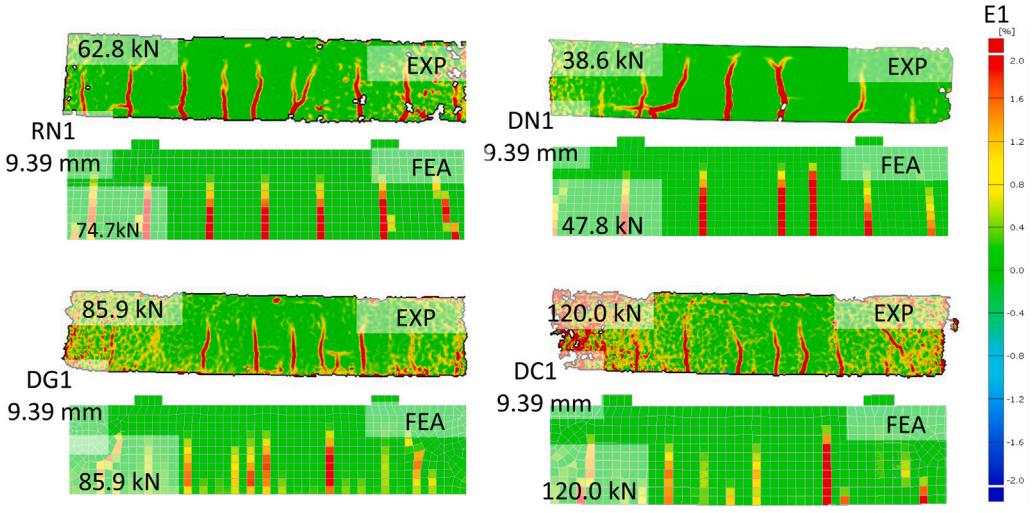

Fig. 12. Comparison of crack pattern from tests (DIC results) and FE analyses. E1 is the main tensile strain. Shown here are the RN1 - reference beam; DN1 - damaged but non-strengthened beam; DG1 - strengthened with GFRP sheet and U-wraps; and DC1 - strengthened with CFRP sheet and U-wraps..

the cross-sectional area of one neighbouring element on both sides of major pits on rebar I and II of DN1 beam. The FE analyses of the DN1PE_FEA model resulted in that the rupture of the rebars not happening simultaneously, see Fig. 13. It may be noted that in these analyses, pitting corrosion was present only where the bending moment was constant, and thus, the weakest section determined the capacity.

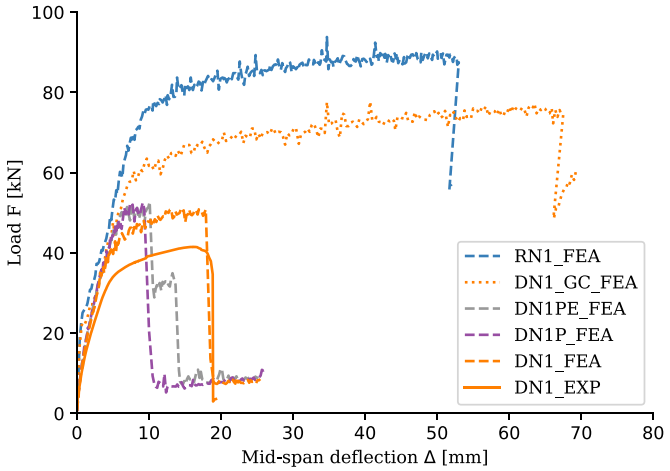

Fig. 13. Load deflection curves for the DN1 beam with different corrosion modelling, compared to test results. Shown here are the RN1_FEA - analysis of reference beam; DN1_GC_FEA - reference beam modified to damaged beam with general corrosion corresponding to DN1 beam; DN1PE_FEA - analysis with extended yield length; DN1P_FEA - analysis with only one major pit in each bar at a critical section; DN1_FEA - the analysis with three major pits in each tensile rebar; DN1_EXP - experimental results of DN1 beam.

For load cases with varying bending moment, it may be necessary to include more corrosion pits to ensure that the behaviour is described correctly.

4.3. Flexural strengthening with GFRP sheet

When analysing the beams strengthened with GFRP (category DG1), it was found that applying GFRP plate at the beam soffit increased the load capacity of the damaged beam to 94.5 kN. This further increased to 111 kN after inclined U-jackets were applied at the end of GFRP sheet on the soffit, see Table 1. The failure modes changed depending on how many FRP components were applied. When only the GFRP sheet was applied, the failure was caused by concrete separation due to high tensile forces at the ends of the sheet (model DG1S_FEA). Meanwhile, applying the inclined U-jackets changed the failure mode to anchorage failure (model DG1I_FEA). The utilisation of the GFRP sheet was 54% for model DG1S_FEA; this increased to 71% after applying inclined U-jackets at the end of GFRP sheet, with non-linear interface properties between FRP connections (model DG1I_FEA).

The stiffness of the beams under the DG1 category was affected significantly by the stiffness of the U-jackets and also the interface properties between the GFRP sheet and the U-jackets. When the intermediate vertical U-jackets were modelled to the GFRP sheet with non-linear interface properties (see Section 3.6), premature failure of the beam occurred due to anchorage failure of the GFRP sheet (model DG1NLI_FEA). This did not correspond with the experimental results. Thus, non-linear interface properties between the inclined U-jackets and the GFRP sheet might be conservative. However, when linear interface properties were used, the failure mode changed to GFRP sheet rupture. In other words its strength was fully utilised (model DG1_FEA), consistent with the experimental results. The assumption of linear interface properties between the inclined U-jackets and the GFRP sheet was accepted due to; (i) the interface properties from Lu et al. [28] was considered to be too conservative, as it is meant for a connection between concrete and FRP, not between FRPs, (ii) relatively low slip values at the ends of the GFRP sheet (see Fig. 14).

4.4. Flexural strengthening with CFRP plate

Fig. 15(a) shows the load versus mid-span deflection curves for different FRP strengthening alternatives. Furthermore, the strain in the CFRP plate was plotted against the mid-span deflection to see the utilisation of CFRP plate in each strengthening configuration, see Fig. 15(b). Moreover, the ultimate load-capacity and corresponding mid-span deflection are presented in Table 1. The application of CFRP plate at the beam soffit increased the load capacity of the damaged beam from 50.8 kN to 119 kN. This further increased to 160 kN after applying inclined U-jackets at the end of CFRP plate on the soffit, see Table 1.

For the beam in category DC1, the CFRP plate had relatively high stiffness compared to the U-jackets and acted as the main load-carrying member. Therefore, the behaviour of the DC1 beam was less influenced by the connection between the CFRP plate and U-jackets, compared to the beams in category DG1. Thus, non-linear interface properties were successfully implemented. The stiff CFRP plate had brittle anchorage failure, limiting the utilisation of its high tensile strength. The inclined U-jackets delayed the anchorage failure of the CFRP plate by providing extra anchorage to its end. With a mesh size of 5 mm, it was possible to capture the stress concentrations in the interface at the end of the CFRP plates. In an additional analysis of DC1, equivalent to DC1_FEA but with a coarse mesh for the CFRP, high stress concentrations resulted in a premature anchorage failure of the CFRP plate. The utilisation of the CFRP plate was 28% for the beam with CFRP plate only. This increased to 41% after applying inclined U-jackets at the end of CFRP plate. It is interesting to note that applying intermediate U-jackets had negligible influence on load and deformation capacity for the beam with CFRP plate at soffit. This might be because the CFRP plate has high stiffness compared to U-jackets, and corrosion cracks were localised only in mid zone. In other words, corrosion cracks did not extend all the way in the studied beam. This may also be taken to mean that the inclined and vertical U-jackets were not mobilised effectively in the experiments. For cases with corrosion-induced cracks present in a larger part of the span, the vertical U-jackets may be of larger importance. It can be noted that in analyses of such cases, it will be important to properly describe the effect of corrosion-induced cracks on bond and anchorage [13]. This requires further research.

4.5. Discussion

The structural behaviour of strengthened beams with corroded reinforcement is complex, and thus, analyses must include a sufficient level of complexity. In the analyses presented, modelling of pitting corrosion, was important. Further, the interface properties, between FRP-to-concrete and between the FRPs, influenced to some extent. Modelling of corrosion-induced cracking did not influence the results to any major extent in most of the analyses; this was concluded as the presence of vertical U-jackets did not make any major difference. However, modelling of the corrosion-induced cracks most likely affected the results in the analysed case exhibiting concrete separation as failure mode (analysis DG1S_FEA). Further, as shown experimentally, intermediate U-jackets contribute for other configurations [8]. Thus, it is considered important to include the effect of corrosion-induced cracks in analyses of strengthened beams with corroded reinforcement. Further, the effect of corrosion-induced cracks on bond and anchorage was not of importance in the analysed cases but should be included when that is critical [13].

5. Conclusions

In this work, finite element analyses were carried out to study corrosion-damaged RC beams strengthened with externally bonded FRP composites. From this work, the following conclusions were drawn:

- Non-linear finite element analysis were able to predict the structural behaviour of damaged and strengthened RC beams. The FE analyses were useful in studying the effects of the different parts of the applied FRP composites.

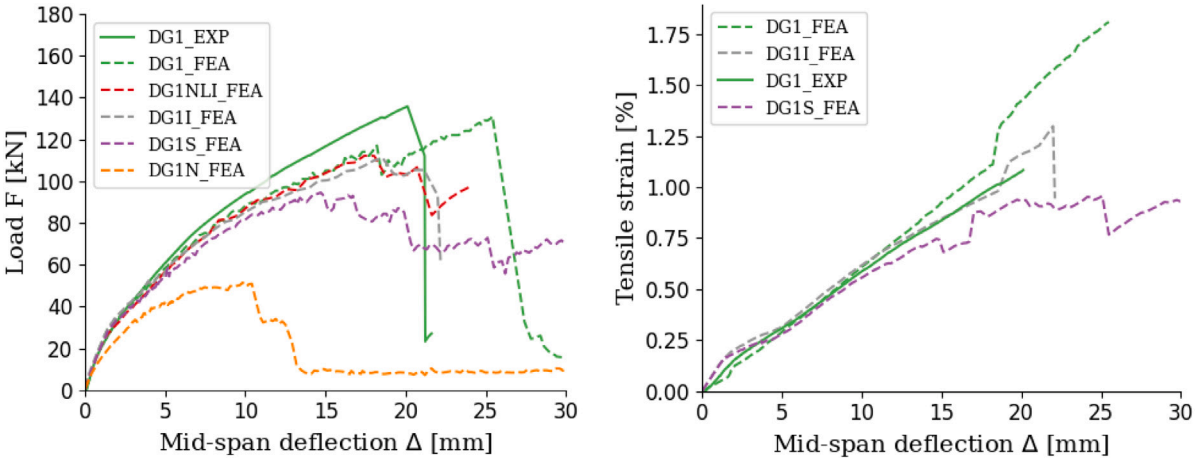

Fig. 14. (a) Load versus mid-span deflection curves for DG1 beam with different strengthening alternatives. (b) Strain at an integration point corresponding to the critical section of GFRP sheet vs mid-span deflection. Shown here are the DG1_EXP - experimental result; DG1_FEA - strengthened with GFRP sheet, inclined U - jackets and vertical U - jackets with linear interface properties between vertical U - jackets and GFRP sheet; DG1NLI_FEA - strengthened with GFRP sheet, inclined U-jackets and vertical U-jackets with non-linear interface properties between vertical U-jackets and GFRP sheet; DG1I_FEA - strengthened with GFRP sheet and inclined U-jackets; DG1S_FEA - strengthened with GFRP sheet; and DG1N_FEA - analysis of non-strengthened beam.

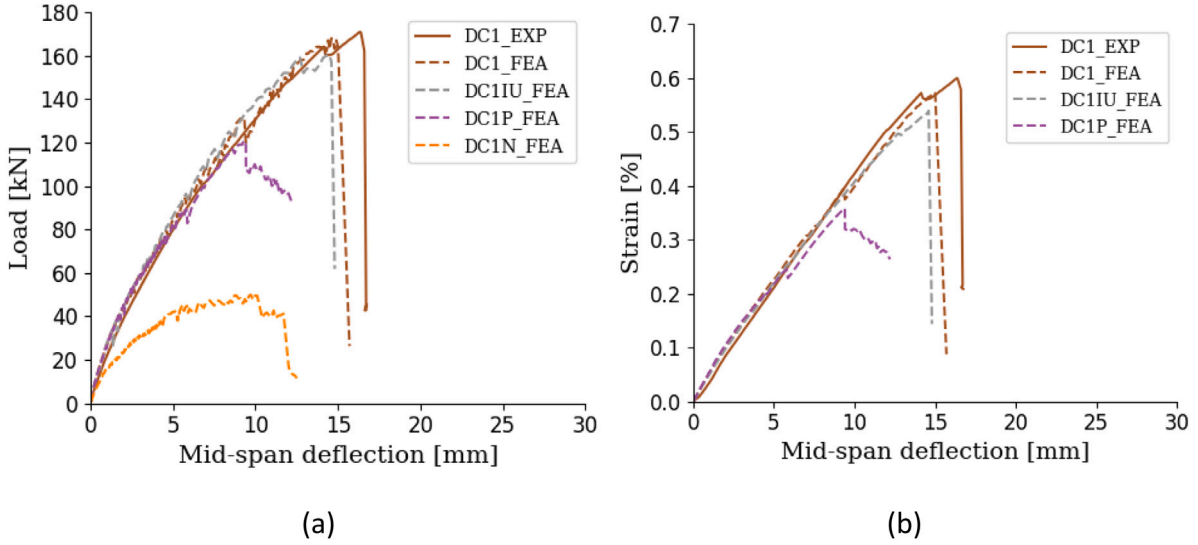

Fig. 15. (a) Load vs mid-span deflection curves for DC1 beam with different strengthening alternatives. (b) Strain at an integration point corresponding to mid-span section vs mid-span deflection. Shown here are the DC1_EXP - experimental result; DC1_FEA - strengthened with CFRP plate, inclined U-jackets and vertical U-jackets; DC1IU_FEA - strengthened with CFRP plate and inclined U-jackets; DC1P_FEA - strengthened with CFRP plate; and DC1N_FEA - analysis of non-strengthened.

- The pitting corrosion majorly influenced the load and deformation capacity, while the average corrosion had a lesser effect on the load capacity and did not influence deformation capacity.
- Modelling of the corrosion pits was highly influential and crucial in predicting the deformation capacity and failure mode of the beam. However, the ultimate load remained unaffected regardless of how the pits were modelled.
- Strengthening significantly increased the ultimate load capacity and stiffness of the corrosion-damaged RC beams. The application of FRP effectively suppressed the opening of cracks.
- For the studied beam geometry and corrosion damage, strengthening with intermediate vertical U-jackets did not further improve the flexural performance of the damaged beams with CFRP plate at the beam soffit.
- The interface properties between FRP-to-concrete and between the FRPs in the FE model were important in accurately predicting the load-carrying capacity and failure mode of the strengthened beams. The interface properties between the GFRP sheet and U-jackets were more influential in predicting the flexural behaviour of the GFRP-strengthened beam than the interface properties between the CFRP plate and U-jackets.

This work forms the basis for FE analyses of corrosion-damaged concrete beams strengthened with FRP, and was validated with well-defined experiments. The developed modelling technique may be used to further evaluate the effectiveness of strengthening methods in parameter studies, including beams of varying dimensions, corrosion patterns and levels, and spacing and dimensions of FRP. In the current study, corrosion-induced cracks were located in mid-region only, and even if the cracks were up to 1.9 mm wide, no spalling was included. It would be interesting to analyse specimens with corrosion-induced cracks extending up to the beam supports and investigate whether this would increase the demand for intermediate vertical U-jackets. For practical applications, it is also worth noting that detailed knowledge of the corrosion pits is of major importance to proper modelling. However, this information is very difficult to obtain for existing structures. Thus, a reliable and efficient damage detection technique, providing accurate information about pitting corrosion, would be of major benefit in assessing existing structures.

CRediT authorship contribution statement

Milan Gotame: Conceptualization, Methodology, Software, Validation, Formal analysis, Investigation, Data curation, Writing – original draft, Visualization. **Carl Lindqvist Franklin:** Methodology, Software, Validation, Formal analysis, Investigation, Data curation. **Mattias Blomfors:** Methodology, Writing – review & editing, Supervision. **Jincheng Yang:** Conceptualization, Methodology, Writing – review & editing, Supervision. **Karin Lundgren:** Conceptualization, Methodology, Validation, Writing – review & editing, Supervision, Project administration, Funding acquisition.

Declaration of competing interest

The authors declare that they have no known competing financial interests or personal relationships that could have appeared to influence the work reported in this paper.

Acknowledgments

This work was financially supported by the Swedish Transport Administration [grant number BBT-2018-011]. The computations were performed on resources at the Chalmers Centre for Computational Science and Engineering (C3SE) provided by the Swedish National Infrastructure for Computing (SNIC).

References

[1] Al-Mahaidi R, Kalfat R. Introduction. In: Rehabilitation of concrete structures with fiber-reinforced Polymer, no. 2004. Matthew Deans; 2018, p. 1–5. http://dx.doi.org/10.1016/b978-0-12-811510-7.00001-x.

[2] Zhou Y, Gencturk B, Willam K, Attar A. Carbonation-induced and chloride-induced corrosion in reinforced concrete structures. J Mater Civ Eng 2015;27(9):04014245. http://dx.doi.org/10.1061/(asce)mt.1943-5533.0001209.

[3] Fernandez I, Herrador MF, Marí AR, Bairán JM. Structural effects of steel reinforcement corrosion on statically indeterminate reinforced concrete members. Mater Struct/Mater Construct 2016;49(12):4959–73. http://dx.doi.org/10.1617/s11527-016-0836-2.

[4] Chen E, Berrocal CG, Fernandez I, Löfgren I, Lundgren K. Assessment of the mechanical behaviour of reinforcement bars with localised pitting corrosion by digital image correlation. Eng Struct 2020;219(May):110936. http://dx.doi.org/10.1016/j.engstruct.2020.110936.

[5] Lundgren K. Bond between ribbed bars and concrete. Part 1: Modified model. Mag Concr Res 2005;57(7):371–82. http://dx.doi.org/10.1680/macr.2005.57.7.371.

[6] Al-Mahaidi R, Kalfat R. Methods of structural rehabilitation and strengthening. In: Rehabilitation of concrete structures with fiber-reinforced polymer, no. 2004. Matthew Deans; 2018, p. 7–13. http://dx.doi.org/10.1016/b978-0-12-811510-7.00002-1.

[7] Hawileh RA, Rasheed HA, Abdalla JA, Al-Tamimi AK. Behavior of reinforced concrete beams strengthened with externally bonded hybrid fiber reinforced polymer systems. Mater Des 2014;53:972–82. http://dx.doi.org/10.1016/j.matdes.2013.07.087.

[8] Al-Saidy AH, Al-Jabri KS. Effect of damaged concrete cover on the behavior of corroded concrete beams repaired with CFRP sheets. Compos Struct 2011;93(7):1775–86. http://dx.doi.org/10.1016/j.compstruct.2011.01.011.

[9] Al-Saidy AH, Saadatmanesh H, El-Gamal S, Al-Jabri KS, Waris BM. Structural behavior of corroded RC beams with/without stirrups repaired with CFRP sheets. Mater Struct/Mater Construct 2016;49(9):3733–47. http://dx.doi.org/10.1617/s11527-015-0751-y.

[10] Bergström M. Assessment of existing concrete bridges. Bending stiffness as a performance indicator [Ph.D. thesis], Luleå University of Technology; 2009, p. 248, http://urn.kb.se/resolve?urn=urn:nbn:se:ltu:diva-26096.

[11] Triantafyllou GG, Rousakis TC, Karabinis AI. Effect of patch repair and strengthening with EBR and NSM CFRP laminates for RC beams with low, medium and heavy corrosion. Composites B 2018;133:101–11. http://dx.doi.org/10.1016/j.compositesb.2017.09.029.

[12] Blomfors M, G. Berrocal C, Lundgren K, Zandi K. Incorporation of pre-existing cracks in finite element analyses of reinforced concrete beams without transverse reinforcement. Eng Struct 2021;229:111601. http://dx.doi.org/10.1016/j.engstruct.2020.111601.

[13] Blomfors M, Lundgren K, Zandi K. Incorporation of pre-existing longitudinal cracks in finite element analyses of corroded reinforced concrete beams failing in anchorage. Struct Infrastruct Eng 2020;1–17. http://dx.doi.org/10.1080/15732479.2020.1782444.

[14] Yang J, Haghani R, Blanksvärd T, Lundgren K. Experimental study of FRP-strengthened concrete beams with corroded reinforcement. Constr Build Mater 2021;301:124076. http://dx.doi.org/10.1016/j.conbuildmat.2021.124076.

[15] Biondini F, Vergani M. Deteriorating beam finite element for nonlinear analysis of concrete structures under corrosion. Struct Infrastruct Eng 2015;11(4):519–32. http://dx.doi.org/10.1080/15732479.2014.951863.

[16] Belletti B, Damoni C, Hendriks MA, de Boer A. Validation of the Guidelines for Nonlinear Page 2 of 129 Finite Element Analysis of Concrete Structures. June, 129. 2017, https://homepage.tudelft.nl/v5p05/RTD%201016-3C(2017)%20version%201.0%20Validation%20of%20the%20guidelines%20for%20NLFEA%20of%20RC%20structures%20Part%20Slabs.pdf.

[17] Mathern A, Yang J. A practical finite element modeling strategy to capture cracking and crushing behavior of reinforced concrete structures. Materials 2021;14(3):1–26. http://dx.doi.org/10.3390/ma14030506.

[18] Kodur VK, Bhatt PP. A numerical approach for modeling response of fiber reinforced polymer strengthened concrete slabs exposed to fire. Compos Struct 2018;187(November 2017):226–40. http://dx.doi.org/10.1016/j.compstruct.2017.12.051.

[19] Blomfors M, Zandi K, Lundgren K, Coronelli D. Engineering bond model for corroded reinforcement. Eng Struct 2018;156:394–410. http://dx.doi.org/10.1016/j.engstruct.2017.11.030.

[20] Earij A, Alfano G, Cashell K, Zhou X. Nonlinear three–dimensional finite–element modelling of reinforced–concrete beams: Computational challenges and experimental validation. Eng Fail Anal 2017;82(September):92–115. http://dx.doi.org/10.1016/j.engfailanal.2017.08.025.

[21] Hawileh RA, El-Maaddawy TA, Naser MZ. Nonlinear finite element modeling of concrete deep beams with openings strengthened with externally-bonded composites. Mater Des 2012;42:378–87. http://dx.doi.org/10.1016/j.matdes.2012.06.004.

[22] Hawileh RA. Nonlinear finite element modeling of RC beams strengthened with nsm FRP rods. Constr Build Mater 2012;27(1):461–71. http://dx.doi.org/10.1016/j.conbuildmat.2011.07.018.

[23] Kalfat R, Al-Mahaidi R. Numerical and experimental validation of FRP patch anchors used to improve the performance of FRP laminates bonded to concrete. J Composit Construct 2014;18(3):1–10. http://dx.doi.org/10.1061/(asce)cc.1943-5614.0000437.

[24] Cui S, Wang J, Shi L, Liu Y. Test and FEM analysis of debonding failure of RC beam strengthened with CFRP. J Reinf Plast Compos 2009;28(17):2151–60. http://dx.doi.org/10.1177/0731684408091932.

[25] Wu YF, Wang Z, Liu K, He W. Numerical analyses of hybrid-bonded FRP strengthened concrete beams. Comput-Aided Civ Infrastruct Eng 2009;24(5):371–84. http://dx.doi.org/10.1111/j.1467-8667.2009.00596.x.

[26] Freddi F, Savoia M. Analysis of FRP-concrete debonding via boundary integral equations. Eng Fract Mech 2008;75(6):1666–83. http://dx.doi.org/10.1016/j.engfracmech.2007.05.016.

[27] Lu XZ, Ye LP, Teng JG, Jiang JJ. Meso-scale finite element model for FRP sheets/plates bonded to concrete. Eng Struct 2005;27(4):564–75. http://dx.doi.org/10.1016/j.engstruct.2004.11.015.

[28] Lu XZ, Teng JG, Ye LP, Jiang JJ. Bond-slip models for FRP sheets/plates bonded to concrete. Eng Struct 2005;27(6):920–37. http://dx.doi.org/10.1016/j.engstruct.2005.01.014.

[29] Chen GM, Chen JF, Teng JG. On the finite element modelling of RC beams shear-strengthened with FRP. Constr Build Mater 2012;32:13–26. http://dx.doi.org/10.1016/j.conbuildmat.2010.11.101.

[30] Anıl Ö, Durucan C, Emin M, Özge Baeğmez K, Kara ME, Baeğmez O. Nonlinear three-dimensional FE analyses of RC beams retrofitted using externally bonded CFRP sheets with or without anchorages. Composites Part B: Engineering 2017;31(7):770–86. http://dx.doi.org/10.1080/01694243.2016.1232040.

[31] Hawileh RA, Musto HA, Abdalla JA, Naser MZ. Finite element modeling of reinforced concrete beams externally strengthened in flexure with side-bonded FRP laminates. Composites B 2019;173(May):106952. http://dx.doi.org/10.1016/j.compositesb.2019.106952.

[32] Yang J. Strengthening reinforced concrete structures with FRP composites [Ph.D. thesis], Chalmers University of Technology; 2021, https://research.chalmers.se/publication/522501.

[33] TNO DIANA. DIANA 10.4. users manual 2020. In: DIANA FEA. 2020, URL https://dianafea.com.

[34] Hendriks MA, de Boer A, Belletti B. Guidelines for nonlinear finite element analysis of concrete structures: Girder members - report RTD:1016:2012. 2012.

[35] Rots JG. Computational modeling of concrete fracture. 1988, http://resolver.tudelft.nl/uuid:06985d0d-1230-4a08-924a-2553a171f08f.

[36] Cornelissen H, Hordijk D, Reinhardt H. Cornelissen, hordijk, reinhardt - 1986.pdf. 1986, p. 45–56, Heronjournal.Nl, URL http://heronjournal.nl/31-2/6.pdf.

[37] Feenstra PH. Computational aspects of biaxial stress in plain and reinforced concrete. [Ph.D. thesis], Delft University of Technology; 1993, http://resolver.tudelft.nl/uuid:faf2fd16-1c43-4711-b783-9e8e00d10c21.

[38] Vecchio FJ, Collins MP. Compression response of cracked reinforced concrete. 1995, http://dx.doi.org/10.1061/(ASCE)0733-9445(1995)121:7(1153.x).

[39] Franklin C, Gotame M. FE analyses of strengthened concrete beams with corroded reinforcement [M.Sc. thesis], Chalmers University of Technology; 2021, https://hdl.handle.net/20.500.12380/302745.

[40] FIB. Fib model code for concrete structures 2010. 2010.

[41] Wittmann FH, Rokugo K, Brühwiler E, Mihashi H, Simonin P. Fracture energy and strain softening of concrete as determined by means of compact tension specimens. Mater Struct 1988;21(1):21–32. http://dx.doi.org/10.1007/BF02472525.

[42] Lundgren K. Bond between ribbed bars and concrete. Part 2: The effect of corrosion. Mag Concr Res 2005;57(7):383–95. http://dx.doi.org/10.1680/macr.2005.57.7.383.

[43] Jiradilok P, Nagai K, Matsumoto K. Meso-scale modeling of non-uniformly corroded reinforced concrete using 3D discrete analysis. Eng Struct 2019;197(April):109378. http://dx.doi.org/10.1016/j.engstruct.2019.109378.